Dalton Transactions

ROYAL SOCIETY OF CHEMISTRY

PAPER

View Article Online
View Journal

Cite this: DOI: 10.1039/d5dt02838h

Ni(II)-oxalate on plastic-derived carbon: a green platform for furfural diacetal synthesis

Alexander Pokutsa,[a] Salvador Perez-Huertas,[a] Alina Mariana Balu *[a] and Rafael Luque *[b,c]

Received 27th November 2025,
Accepted 13th January 2026

DOI: 10.1039/d5dt02838h

rsc.li/dalton

An efficient and environmentally benign method for the synthesis of diacetals from furfural (FF) and heavy aliphatic (1-hexanol) or alicyclic (cyclohexanol) alcohols is reported for the first time. A novel catalyst comprising 2.5 wt% Ni(II) oxalate deposited on carbon char derived from the pyrolysis of plastic waste was synthesized and employed under microwave-assisted conditions. The catalyst effectively promoted the acetalization of FF with heavy alcohols at 130–170 °C, achieving up to 70% FF conversion and 99% selectivity toward diacetals within one hour in both binary (FF + single alcohol) and ternary (FF + mixed alcohols) systems. Reactions involving mixed alcohols resulted in a notable 40–50% increase in total productivity, yielding furfurylhexyl diacetal, furfurylcyclohexyl diacetal, and the hybrid furfurylhexyl/cyclohexyl diacetal. The addition of *n*-hexane as a co-solvent further enhanced yields, particularly at lower temperatures and when using the sterically hindered secondary alcohol (cyclohexanol). Under optimized conditions (150–170 °C, 40–45 vol% *n*-hexane), the yield of furfurylcyclohexyl diacetal increased five- to sixfold compared with reactions conducted in the absence of co-solvent. These findings highlight the catalytic potential of plastic-derived Ni(II) oxalate/carbon systems for sustainable diacetal synthesis from biomass-derived aldehydes.

Introduction

The reaction between aldehydes or ketones and alcohols (acetalization/ketalization) yields diacetals, which are widely used as protective groups to shield carbonyl functionalities during the synthesis of temperature-sensitive compounds such as steroids, carbohydrates, and intermediates for organic pigments. In addition, diacetals have broad applications in the production of foods, tobacco, fragrances, flavors, pharmaceuticals, and agrochemicals.[1–4] An alternative utilization route involves the hydrogenation of acetals to produce ethers (including furan-derived ethers) and the corresponding alcohols, typically catalyzed by Lewis acids.[5–7] According to the mechanism of aldehyde acetalization (Scheme 1), formation of the diacetal proceeds *via* the addition of a second alcohol molecule to the hemiacetal intermediate, followed by deprotonation. This step occurs concurrently with water elimination and does not involve the loss of H^+ or reformation of the carbonyl group.[8]

Homogeneous Brønsted acids such as HCl, H_2SO_4, H_3PO_4, and *p*-toluenesulfonic acid have been traditionally employed as catalysts for these type of reactions.[9–11] However, the widespread use of toxic, corrosive, and non-recoverable acids poses serious environmental concerns, prompting their gradual replacement with solid Lewis acids, graphene oxide (which also contains Lewis acidic sites), and more recently, bio-inspired or enzymatic acid catalysts.[7,12,13] Heterogeneous catalysts—typically comprising noble metals (*e.g.*, Ru, Pt, Pd) or non-noble metals (*e.g.*, Co, Ni, Cu, Mo, V, Zn)—are commonly dispersed on inorganic supports such as silicate clays, aluminophosphates, mesoporous silicas, and zeolites, or on organic supports such as synthetic polymers and resins.[14,15] The selection of an appropriate support is critical, as it dictates the dis-

[a]*Universidad de Córdoba, Departamento de Química Orgánica, Campus de Rabanales, Edificio Marie Curie (C-3), Carretera Nacional IV-A, Km. 396, E14014 Cordoba, Spain. E-mail: qo2balua@uco.es*
[b]*Universidad ECOTEC, Km. 13.5 Samborondón, Samborondón, EC092302, Ecuador*
[c]*Department of Bioresources and Polymer Science, Advanced Polymer Materials Group, Faculty of Chemical Engineering and Biotechnologies, National University of Science and Technology Polytehnica Bucharest, 1-7 Gheorghe Polizu str., Bucharest, Romania*

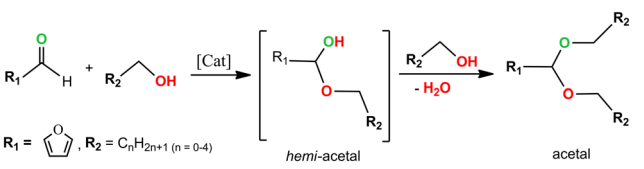

Scheme 1 The main route of aldehyde transformation into acetals by the reaction with alcohols.

persion, accessibility, and stability of the active catalytic species.

In recent years, catalyst supports derived from waste plastics have attracted growing attention due to both environmental and economic imperatives. Global plastic production now exceeds 400 million tons annually and is expected to approach one billion tons by 2050.[16] Most of these materials are non-biodegradable, and their accumulation in landfills and natural ecosystems has made them among the most persistent and hazardous organic pollutants worldwide. Consequently, significant research efforts have focused on developing sustainable strategies for plastic valorization. Among the various approaches, pyrolysis has emerged as an efficient route for converting plastic waste into valuable products such as gases, oils, and solid carbonaceous materials (char).[17] Pyrolyzed plastic char is particularly attractive owing to its high carbon content, adjustable porosity, and surface functionality. Its use as a support for heterogeneous catalysts offers a promising means to improve catalyst stability, reusability, and performance while simultaneously contributing to plastic waste mitigation.[18] Thus, plastic-derived carbon char represents a sustainable and versatile platform for catalytic applications, including the valorization of biomass-derived compounds such as furfural (FF).[19]

The catalytic conversion of biomass-derived platform molecules provides an efficient pathway to reduce dependence on fossil resources, owing to their high degree of functionalization. Among these, furan-based derivatives—particularly furfural (FF)—serve as versatile building blocks for diverse transformations, including alkylation, hydrogenation, oxidation, halogenation, and nitration. These reactions yield valuable intermediates such as furan, methylfuran, furfurylamine, and furoic acid, which are crucial precursors for pharmaceuticals, fuels, fine chemicals, and polymeric materials.

In recent years, the synthesis of diacetals has gained increasing industrial attention, primarily due to their potential use as additives in diesel and jet fuels.[20] Furfural-based acetals with higher (C_4^+) alcohols are particularly attractive as fuel improvers. Their incorporation into fuel blends enhances lubricity, widens the boiling range, increases oxidation resistance, and improves the cetane number, while simultaneously reducing CO, CO_2, NO_x, and SO_x emissions. When derived from renewable feedstocks through sustainable catalytic processes, such additives represent a promising route toward next-generation, environmentally friendly fuels.

Traditionally, diacetal synthesis relies on catalysts containing noble metals such as Ru, Pt, or Pd.[14] However, due to the high cost and limited availability of these materials, research has increasingly focused on more affordable transition metals such as Co, Ni, Cu, Zr, Mo, V, and Zn.[15] For example, Fe- and Co-oxalate catalysts supported on silica have shown notable activity in furfural acetalization reactions.[21] Their efficiency likely arises from the coexistence of Brønsted and mild Lewis acid sites on the surface—originating from both oxalate species and the support—which are essential for promoting the acetalization pathway.

In this context, we report the sustainable synthesis of a novel Ni(II) oxalate-based catalyst supported on carbon char derived from plastic waste (NiOx@CSR) and its evaluation in the acetalization of bio-based furfural with C_6 alcohols. The catalyst, containing 2.5 wt% Ni(II) oxalate, was thoroughly characterized and tested under microwave-assisted conditions (130–170 °C) for the production of furfuryl diacetals using both aliphatic (1-hexanol) and alicyclic (cyclohexanol) alcohols, individually and in binary mixtures.

Furthermore, this study introduces a co-solvent strategy in heterogeneous catalysis aimed at tuning the physicochemical properties of the reaction medium to enhance catalytic efficiency. *n*-Hexane, a green and microwave-silent co-solvent, was employed in combination with 1-hexanol or cyclohexanol. The beneficial effects of *n*-hexane are attributed to: (i) reduced viscosity of the reaction medium, which facilitates mass transfer between reactants (FF and alcohols) and the active NiOx sites on the hydrophobic carbon support; and (ii) improved heat distribution under microwave irradiation, minimizing local overheating and subsequent furfural polymerization. While co-solvent use has been occasionally reported in related systems, its deliberate implementation as a design parameter to control catalytic performance remains largely unexplored.

Results and discussion

Catalysts characterization

N_2 adsorption–desorption isotherms and surface morphologies of the pristine carbon support (CSR), NiOx, and the 2.5% NiOx@CSR composite are shown in Fig. 1. According to the IUPAC classification, NiOx exhibits a type IV isotherm (Fig. 1b), typical of mesoporous materials, consistent with its average pore diameter of 25 nm and pore volume of 0.644 $cm^3 g^{-1}$. In contrast, the CSR support displays an isotherm characteristic of non-porous materials, such as unactivated carbon chars (Fig. 1a), with a very low specific surface area (<10 $m^2 g^{-1}$). The apparent average pore diameter of CSR (71 nm) lies outside the mesoporous range (2–50 nm), which is likely an artefact arising from the calculation method applied to a material with low surface area and poorly developed porosity, rather than evidence of true macroporosity. Indeed, N_2 adsorption–desorption analysis is not reliable for quantifying pores larger than the mesopore domain, and such results should be interpreted cautiously.[22]

This interpretation is supported by SEM micrographs of CSR (Fig. 1d), which show no visible intraparticle porosity. The observed textural voids likely correspond to interparticle gaps —a feature typical of non-activated carbons.[23] NiOx@CSR displays an intermediate adsorption profile (Fig. 1c), combining characteristics of both non-porous and mesoporous materials. Its specific surface area (11 $m^2 g^{-1}$) remains close to that of CSR, while the calculated average pore diameter (40 nm) falls within the mesoporous range, suggesting partial surface coverage by NiOx. As seen in SEM images (Fig. 1f), NiOx nanoparticles are homogeneously dispersed on the CSR surface,

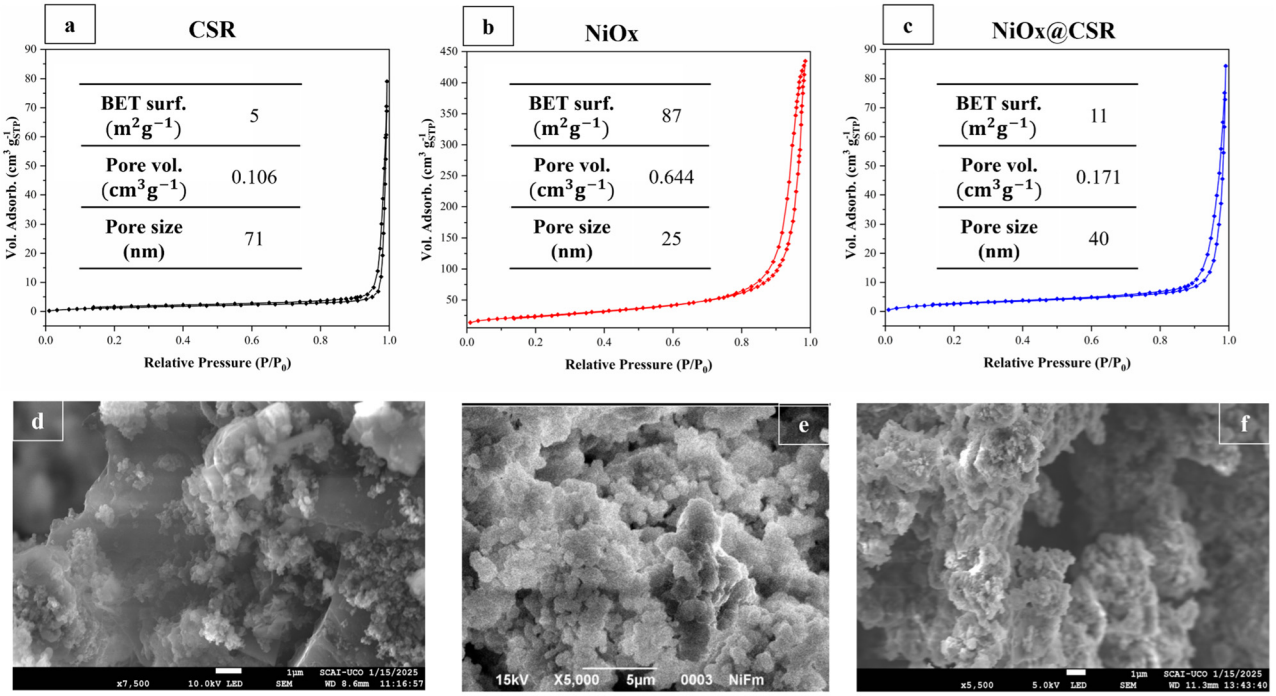

Fig. 1 BET Isotherms and SEM images for: (a and d) CSR, (b and e) NiOx and (c and f) 2.5NiOx@CSR (respectively), including pore properties by BJH.

partially coating the interparticle voids and forming thin, accessible catalytic layers. These surface features likely represent the initial active sites available for molecular adsorption and catalytic interaction. This assumption is supported by the fact that the pore volume of 2.5%NiOx@CSR closely matches that of the pristine CSR, which, as the support, defines most of the final material structure.

The characteristic diffraction peaks corresponding to the CSR, NiOx, and NiOx@CSR catalyst, along with the standard reference peaks for $NiC_2O_4{\cdot}2H_2O$ and $CaCO_3$ phases are presented in Fig. 2.

TheXRD pattern of CSR presents main diffraction peaks at 26° (012), 29° (104), 37° (110), 39° (113), 43° (202), 47° (024), and 48° (018), suggesting the presence of calcium carbonate as one of the compounds that generate the diffraction pattern (JCPDS no. 01-086-0174). The presence of Ca-related diffraction peaks in the XRD pattern of the CSR char can be attributed to the origin of the plastic, *e.g.*, calcium-based additives are com-

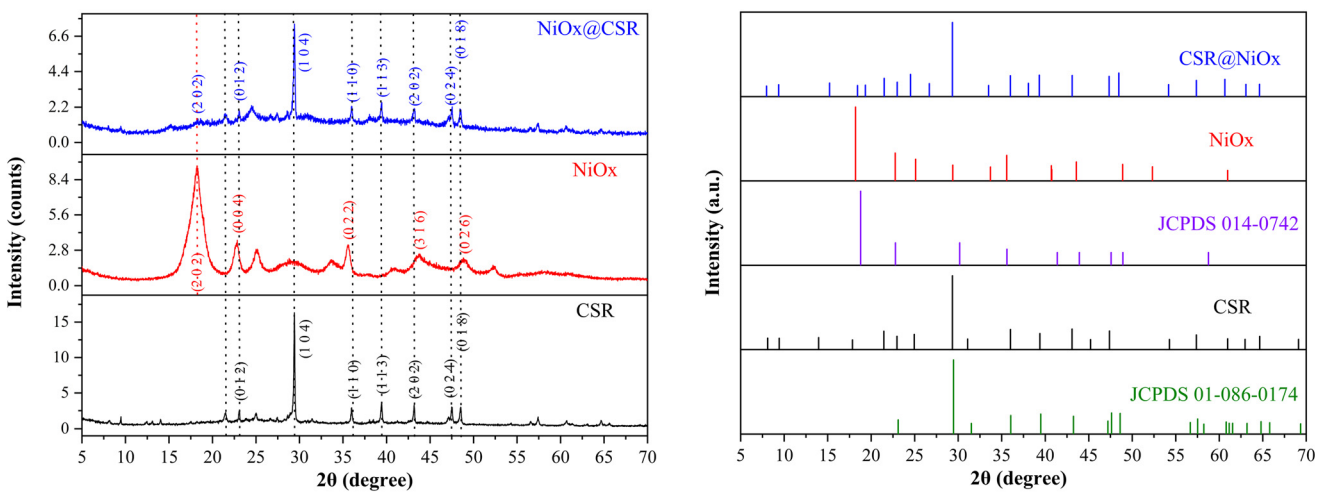

Fig. 2 XRD patterns of the catalyst support (CSR), bulk NiOx and the catalyst (2.5NiOx@CSR) (left). Standard diffraction peaks of $NiC_2O_4{\cdot}2H_2O$ and $CaCO_3$ from JCPDS cards No. 014-0742 and No. 01-086-0174, respectively (right).

monly used in commercial plastics, obtained from municipal waste. In particular, calcium carbonate ($CaCO_3$) is widely employed as a filler in polymers such as polyethylene, polypropylene, polystyrene, and polyvinyl chloride, where it may account for a significant portion of the material weight. Additionally, the presence of Ca in the CSR was also detected by SEM-EDS, which is discussed below (see Table 1).

XRD diffraction pattern of NiOx@CSR (Fig. 2) reveals the coexistence of diffraction peaks corresponding to both the CSR support and the monoclinic phase of nickel(II) oxalate dihydrate (JCPDS No. 014-0742). The presence of reflections from $NiOx{\cdot}2H_2O$ confirms the successful deposition of NiOx species onto the carbon surface. Compared to pristine CSR, 2.5% NiOx@CSR exhibits a slightly reduced degree of crystallinity. This decrease may be attributed to the anchoring of NiOx species onto the active surface sites of CSR during synthesis, which can disrupt the regular stacking of graphitic domains and induce structural disorder. Alternatively, a partial amorphous deposition of NiOx on the surface could also contribute to the diminished crystallinity. However, given the relatively low Ni loading (2.5 wt%), extensive amorphization is unlikely to be the dominant factor.

Elemental mapping by SEM–EDS (Fig. 3) confirms that NiOx particles are uniformly distributed over selected regions of the CSR surface. Quantitative EDS analysis (Table 1) shows a Ni content of approximately 2.2 wt%, in good agreement with the nominal 2.5 wt% target loading. These results verify the successful synthesis of the NiOx@CSR catalyst and indicate that nickel species are predominantly immobilized on the CSR surface in the form of nickel oxalate salts. XPS spectra of CSR and the NiOx@CSR catalyst (Fig. 4) provide detailed insights into the surface composition and oxidation states of the elements present. The Ni 2p region of NiOx@CSR exhibits the characteristic asymmetric peaks of Ni $2p_{3/2}$ and Ni $2p_{1/2}$, accompanied by their respective multiplet and shake-up satellite features, indicative of mixed nickel oxidation states (Fig. 4a).[24,25] Deconvolution of the Ni $2p_{3/2}$ and Ni $2p_{1/2}$ signals reveals four components each, consistent with the coexistence of Ni^{2+} and Ni^{3+} species.[26] The main peaks at ~857 eV correspond to Ni^{2+} from nickel oxalate, while the higher binding energy feature at ~874.3 eV is attributed to Ni^{3+} species formed through partial surface oxidation.[26] These results confirm the presence of NiOx species on the CSR surface.

Further evidence for NiOx deposition is provided by the comparison of the deconvoluted C 1s and O 1s spectra of CSR and 2.5% NiOx@CSR (Fig. 4b). The XPS spectrum of pristine CSR shows a dominant peak at ~284.6 eV, assigned to C–C and C=C bonds characteristic of graphitic carbon.[27] In contrast, the NiOx@CSR composite exhibits additional contributions associated with oxygen-containing functional groups, mainly arising from oxalate species.[28] Specifically, new peaks appear at 286.5 eV (C–O) and 288.5 eV (C=O), while a higher binding energy component at 289.6 eV is attributed to CO_3^{2-} species, likely generated by X-ray–induced decomposition of oxalate, as well as to coordinated oxalate ions ($C_2O_4^{2-}$ or O–C–O groups) bound to the carbon surface.[25,29,30] Collectively, the modifications observed in both the C 1s and Ni 2p regions provide strong evidence for the successful anchoring of NiOx onto the CSR support.

Thermogravimetric analysis (TGA) of the 2.5% NiOx@CSR catalyst (Fig. 5) reveals three main stages of weight loss. The initial mass loss of approximately 10% below 200 °C corresponds to the removal of physically adsorbed moisture and loosely bound water molecules. The second stage, showing a mass loss of about 20% between 400 and 450 °C, is attributed to the thermal decomposition of nickel oxalate. The decomposition process appears nearly complete at around 420 °C, as indicated by the stabilization of the TGA curve beyond this point. Literature reports place the decomposition temperature of nickel oxalate dihydrate in the 350–390 °C range,[30] a process accompanied by the release of H_2O, CO, and CO_2, leading to the formation of NiO as the final product (eqn (1)).[31,32]

$$Ni(HC_2O_4)_2 \rightarrow NiO + 2CO + 2CO_2 + xH_2O \quad (1)$$

The third stage of weight loss, taking place above 450 °C, corresponds to the decomposition of the carbonaceous matrix (CSR), indicating that NiOx@CSR is thermally stable within the reaction temperature range. DTG analysis (Fig. 4b) shows a small peak at 570 °C for the host material, attributed to the breakdown of polycyclic aromatic compounds in the pyrolyzed plastic char. In contrast, NiOx and 2.5%NiOx@CSR exhibit two pronounced mass-loss peaks: 230 °C and 270 °C for NiOx, and 160 °C and 450 °C for 2.5%NiOx@CSR. A minor feature at 60 °C in the latter sample corresponds to the release of physically adsorbed water. Overall, the decomposition profiles are consistent with the material composition and the synthesis procedure. The nature and distribution of acid sites is a key property of catalytic materials, providing valuable insight into their functionality and enabling predictions of performance. Pristine CSR exhibits relatively low total acidity (18 μmol g^{-1}, measured on the basis of previous work from our group[33]), with a slight predominance of Lewis over Brønsted sites (Table 2). Incorporation of NiOx into the support markedly alters the acidity, more than doubling it to 40 μmol g^{-1} in 2.5%NiOx@CSR. This increase is primarily due to a substan-

Table 1 Elemental composition of CSR and 2.5%NiOx@CSR by SEM–EDS

	CSR		2.5%NiOx@CSR	
Element	Wt%	Atomic %	Wt%	Atomic%
C	67.34	78.73	52.93	65.16
O	16.74	14.69	30.57	28.25
Mg	0.99	0.57	0.42	0.26
Al	1.57	0.82	1.78	0.98
Si	3.02	1.51	1.40	0.74
S	0.55	0.24	—	—
Cl	0.25	0.10	2.22	0.92
Ca	9.55	3.34	8,49	3.13
Ni	—	—	2.19	0.55

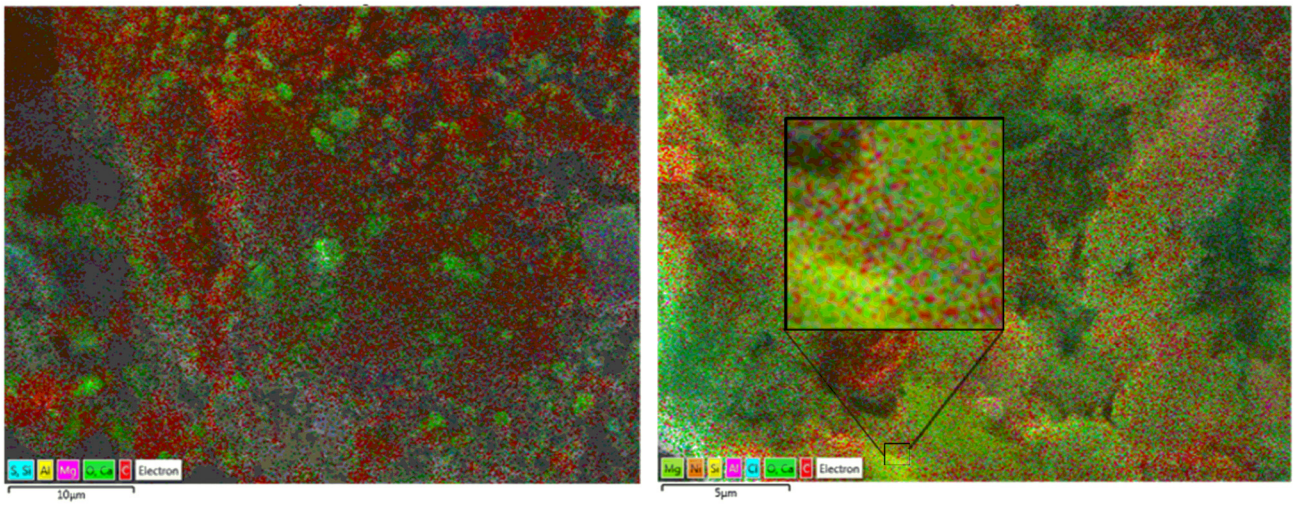

Fig. 3 Elemental mapping of CSR (a) and 2.5%NiOx@CSR (b) by SEM-EDS. The magnified region at b (inset) points out the presence of Ni species (dark-yellow dots). The color of the elements mapped at a corresspponds to the ones at b.

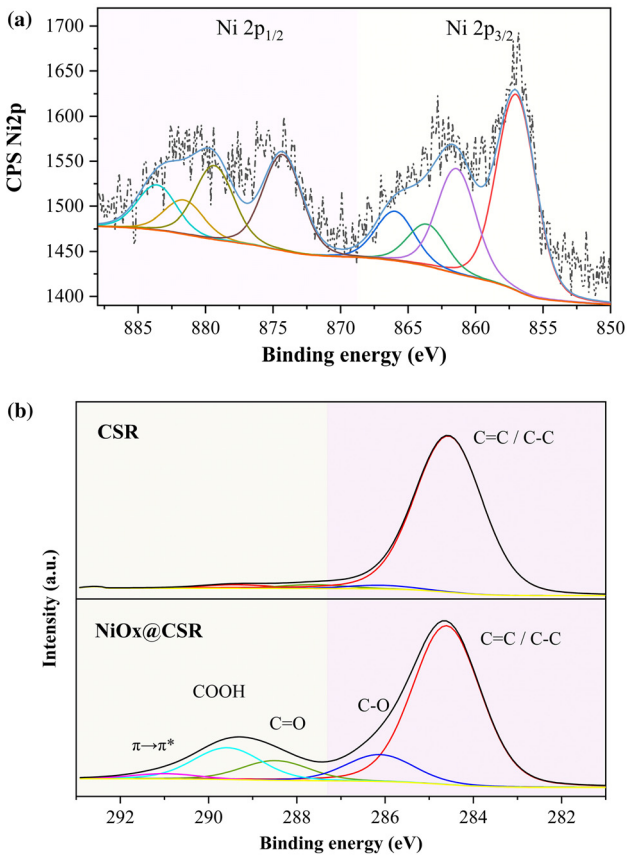

Fig. 4 Deconvoluted XPS Ni 2p spectra of Ni $2p_{1/2}$ and Ni $2p_{3/2}$ (a) and C 1s of C–C and C═C bonds (b) emerged from CSR and 2.5%NiOx@CSR samples.

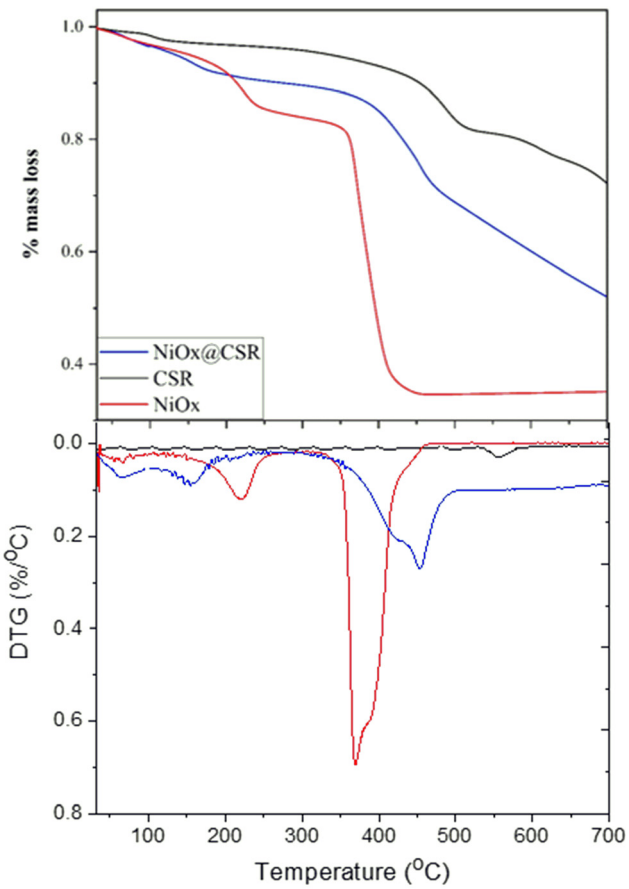

Fig. 5 TG/DTG diagrams of CSR (black), NiOx (red), and the 2.5% NiOx@CSR (blue) samples.

tial rise in Brønsted sites (24 μmol g^{-1}), indicating that NiOx deposition not only introduces additional Lewis acid sites but also promotes Brønsted site formation through interactions with surface oxygenated groups. Ni(II) oxalate (NiOx) displays the highest total acidity (52 μmol g^{-1}), dominated by Lewis sites (70%), consistent with its crystalline nature and absence

Table 2 Acidity of investigated materials[33]

Material	Acidity (μmol g^{-1})			
	Lewis	BrØnsted	BrØnsted + Lewis	BrØnsted sites, %
CSR	10	8	18	43
2.5% NiOx@CSR	16	24	40	60
2.5% NiOx@CSR[a]	<5	12	16	75
NiOx[b]	36	16	52	30

[a] Catalyst collected after FF acetalization reaction (170 °C, 1 h). [b] Bulk Ni(II)oxalate salt.

of carbonaceous functionalities. These results demonstrate that NiOx incorporation significantly enhances the Brønsted acidity of CSR, which is critical for maintaining high catalytic activity in acetalization and related reactions. Furthermore, the observed shift in acidity distribution after four reaction cycles provides insight into the stability and evolution of active sites under operating conditions, as discussed below. The observed activity clearly correlates with acidity, for which the observed decline in catalyst performance after several catalytic cycles (Fig. 8) undoubtedly corresponds to the decreased acidity in the materials (Table 2, values of both BrØnsted and Lewis acidity decreased almost three times).

The surface acidity of the support and catalytic material was also examined using *in situ* Py-DRIFTS, a technique that allows qualitative assessment of the acidic sites of analyzed materials. DRIFTS spectra of adsorbed pyridine revealed the presence of both BrØnsted (1546 cm^{-1}) and Lewis (1446 cm^{-1}) acidic sites, along with a band attributed to the sum of BrØnsted + Lewis (1490 cm^{-1}) acidity (Fig. S1).[33] Lewis (1446 cm^{-1}) and BrØnsted + Lewis (1490 cm^{-1}) sites peaks of bulky Ni(II) oxalate exhibited medium bathochromic shifts compared to CSR and 2.5%NiOx@CSR samples, presumably due to the support surface influence (Fig. S1).

Catalytic tests

The catalytic activity of Ni(II) oxalate deposited on plastic-waste-derived char was evaluated in the acetalization of furfural (FF) with 1-hexanol, cyclohexanol (and mixtures), employed both as reactants and solvents. The reactions were carried out under microwave irradiation at 150–170 °C and atmospheric pressure. In addition to temperature, effects of catalyst loading, reaction time and furfural-to-alcohol molar ratio on process performance were also examined. Fig. 5 summarizes the influence of C6-alcohol composition on FF conversion and selectivity toward the corresponding diacetal products. Although 2.5% NiOx@CSR exhibited high catalytic activity with both alcohols—whether used individually or in mixtures—optimum performance was obtained for 1-hexanol. Blank runs (using the metal-free carbon support (CSR)) exhibited negligible activity (~2% conversion), while bulk NiOx salt containing identical Ni content (2.5% Ni) as in the tested catalytic material achieved less than half conversion as compared to NiOx@CSR under otherwise identical conditions (Table S1). (The impact of $CaCO_3$ impurities, presented in CSR, on the process performance, may be ignored due to the tiny catalytic effect revealed by the pristine CSR). These results illustrate the synergistic effect derived from the uniform dispersion of nickel species on the carbon surface, which enhances both microwave absorption and catalytic efficiency.

FF conversion strongly depends on the alcohol (Fig. 6a). Optimum activity was obtained for 1-hexanol, yielding over 60% conversion and a preferential formation of furfurylhexyl diacetal (99% selectivity). In contrast, reactions with cyclohexanol resulted in substantially reduced conversion (≈25%), producing furfurylcyclohexyl diacetal with complete selectivity (99%) (Fig. 6b). This disparity likely arises from steric and diffusional limitations associated with the cyclic structure of cyclohexanol, which hinders its interaction with both catalyst's

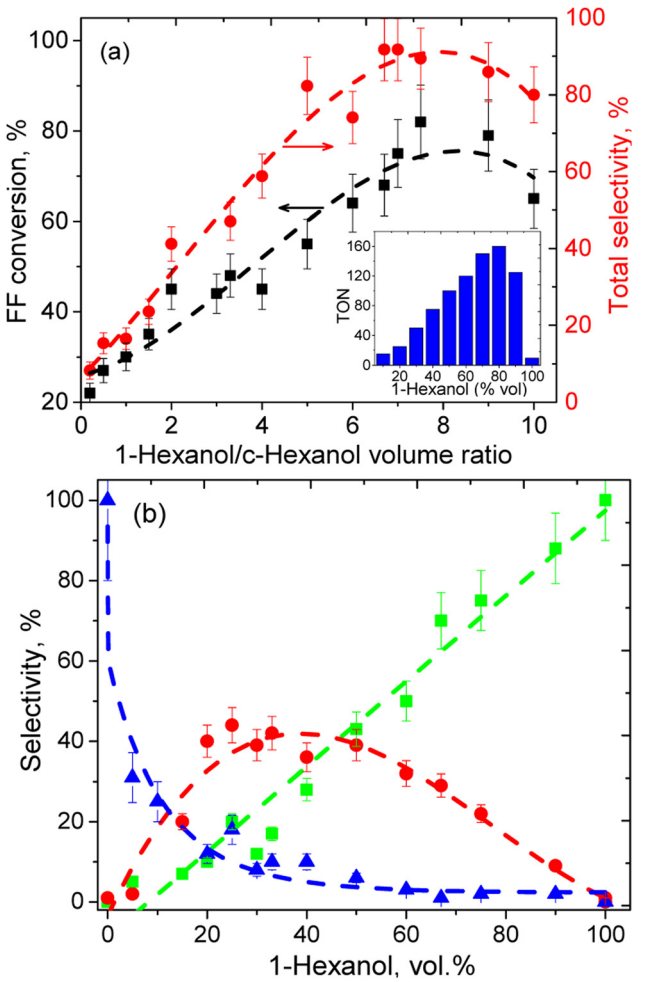

Fig. 6 Impact of (a) 1-hexanol/*c*-hexanol ratio on FF conversion (black squares) and the sum selectivity (red circles) of diacetals and (bottom image) individual diacetals selectivity: furfurylhexyl diacetal (green rectangles), hybrid furfurylhexyl/cyclohexyl diacetal (red circles), furfurylcyclohexyl diacetal (b), 170 °C, 1 h. Inset: dependence of TON values on 1-hexanol/*c*-hexanol ratio.

active sites and FF. GS-MS data available in the ESI confirmed the highly effective formation of furfurylhexyl diacetal (signal at 10.77 min, m/z = 282, Fig. S5) as well as furfurylcyclohexyl diacetal (11.40 min, m/z = 278, Fig. S6) as target products in the reaction.

Interestingly, the acetalization of FF in mixtures of 1-hexanol and cyclohexanol exhibited a remarkable synergistic effect, leading to a significant enhancement in overall performance. The highest FF conversion (≈80%) with >90% combined selectivity toward diacetal products was achieved at a 1-hexanol/cyclohexanol ratio of 0.75 (Fig. 6, top image). A clear preference for the formation of furfurylhexyl diacetal was observed under these conditions (70% selectivity) (Fig. 6, bottom image). In addition, a hybrid furfurylhexyl/cyclohexyl diacetal was detected (35% selectivity), reaching its maximum selectivity (≈45%) at a 1-hexanol-to-cyclohexanol ratio of 0.2–0.3 (Fig. 6b). The formation of this mixed acetal species (peak at 11.038 min, m/z = 280, Fig. S7) represents, to the best of our knowledge, the first report of hybrid furfural diacetals obtained under such conditions. The relative yield of these three products, *i.e.* furfuryl 1-hexyl/furfuryl (*c*-hexyl + 1-hexyl)/furfuryl *c*-hexyl, after reaction followed the order depending on the initial *c*-hexanol/1-hexanol proportions: 1/1.4/0.9 (3/1), 1/1.3/0.8 (2/1), 1/0.9/0.5 (1/1), 1/0.7/0.2 (2/1) and finally 1/0.6/0.2 (3/1) (Fig. S8). Decreasing *c*-hexanol content in the starting mixture led to a decrease in the production of hybride diacetal (in line with simultaneous declining of furfuryl *c*-hexyl diacetal output). At the same time, the overall production of all three products benefits from the increase in 1-hexanol content (Fig. S8). Certainly, such finding pointed out the limiting role of *c*-hexanol as less reactive alcohol in the compound formation mechanism. The discovered features correspond well with the previously discussed relative activity of 1-hexanol and *c*-hexanol in its reaction with FF.

Importantly, the catalytic behavior observed herein differs from previous literature reports, indicating a steady decrease in acetalization activity as the carbon atom number of the alcohol increases above two.[34] In the present case, high conversion (65–70%) and selectivity (90–98%) were obtained even for C6 alcohols, particularly in the case of 1-hexanol (Fig. 6 and Table S1). This result confirms the potential of NiOx@CSR to efficiently promote the studied reaction even with long-chain alcohols.

Optimization experiments revealed that optimum reaction performance could be achieved at 170 °C and a reaction time of 1 h. Increased temperature did not significantly influence the selectivity, suggesting that the produced diacetals are thermally stable under the investigated conditions. Reaction efficiency remained high at elevated temperatures, allowing shorter reaction times without compromising product yields, while extending the reaction beyond 1 h only resulted in a moderate conversion increase (Fig. S2, S3 and Table S1).

To further elucidate the influence of the reaction medium on process performance, additional experiments were carried out using an aliphatic hydrocarbon (*n*-hexane) as microwave-inert co-solvent (the loss tangent value is equal 0.02). Diluting the reaction mixture with this chemically inert solvent may reduce overall viscosity, enhance mass transfer, and improve access of reactant molecules to the catalyst surface. Fig. 7 illustrates the effect of *n*-hexane during the acetalization of FF with 1-hexanol. The addition of *n*-hexane led to a pronounced improvement in catalytic performance while maintaining excellent selectivity toward furfurylhexyl diacetal. At moderate volume ratios (0.1–0.4 relative to 1-hexanol) and at a lower temperature compared to 1-hexanol/cyclohexanol mixture (150 °C *vs.* 170 °C), the reaction yielded from good to excellent FF conversion (up to 70%) with 99% selectivity (Fig. 7a). This enhancement may also result from a favorable adjustment of the reaction-medium polarity, which promotes adsorption–desorption equilibria at the catalyst interface. However, at higher *n*-hexane concentrations, dilution becomes dominant as expected, reducing the effective FF concentration and overall efficiency. A similar, though less pronounced, trend was observed when cyclohexanol was employed as main solvent (Fig. 7b). In the absence of *n*-hexane, FF conversion and

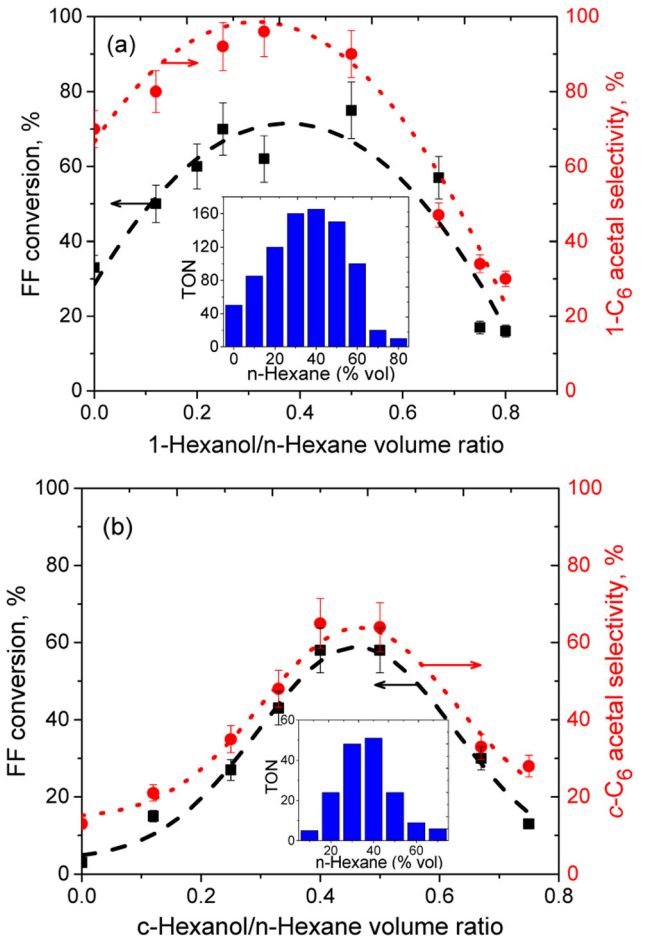

Fig. 7 Impact of diluting agent (*n*-hexane) on the performance of FF acetalization in (a) 1-hexanol medium; 50 mg 2.5%NiOx@CSR, volume 2 mL, 150 °C, 1 h, and (b) in *c*-hexanol medium: 50 mg 2.5%NiOx@CSR, volume 2 mL, 150 °C, 1 h. Insets: dependence of TON values on co-solvent (*n*-hexane) presence.

selectivity were notably low. However, co-solvent addition significantly improved catalytic performance, reaching 60% FF conversion and 60% selectivity toward furfurylcyclohexyl diacetal. The inherently lower reactivity of cyclohexanol—higher steric hindrance—appears to be partially compensated by the improved accessibility of reactants to active centers facilitated by the presence of *n*-hexane. The revealed feature might be rooted in the very small loss tangent value of *n*-Hexane which is certainly below that intrinsic to alcohols, *e.g.* 1-BuOH (0.571),[35] viscosity reduction, polarity modulation and improved water repulsion.

These findings suggest that the physicochemical properties of the solvent, particularly polarity and hydrogen-bonding capacity, partially govern the extent to which co-solvent addition influences the catalytic process. Overall, these results highlight the potential of co-solvent tuning as a strategy to optimize the microenvironment of heterogeneous catalytic systems for biomass-derived transformations. The revealed effect was particularly noticeable at a lower temperature and in case of less reactive *c*-hexanol: for the last one the disclosed tendency was maintained even at 170 °C (compare Fig. 7a *vs.* Fig. S2 and Fig. 7b *vs.* Fig. S3). The effect of 1-hexanol additives to *c*-hexanol on the rate of FF acetalization was mapped in Fig. S4. The 1st derivative (parabolic) dependencies of yield vs 1-hexanol (vol%) indicates a specific dependence on reactant concentrations.

2.5% NiOx@CSR also demonstrated a satisfactory reusability (Fig. 8), with 70–80% of its initial catalytic activity retained after five consecutive catalytic cycles. This behavior underscores the importance of both Brønsted and Lewis acidic sites in sustaining catalytic performance. The high initial activity further aligns with the well-established notion that efficient acetalization catalysts require a balanced distribution of moderate Brønsted and Lewis acid sites.[36] Interestingly, the spent catalyst (2.5% NiOx@CSR-AR) recovered after five cycles exhibited a noticeable decrease in total acidity (16 μmol g^{-1}), along with an increase in the relative proportion of Brønsted sites to 75%. This shift indicates partial deactivation or surface restructuring during the reaction, with Lewis acid sites being more susceptible to deactivation than their Brønsted counterparts. Such evolution of surface acidity likely contributes to the gradual loss of catalytic activity upon recycling.

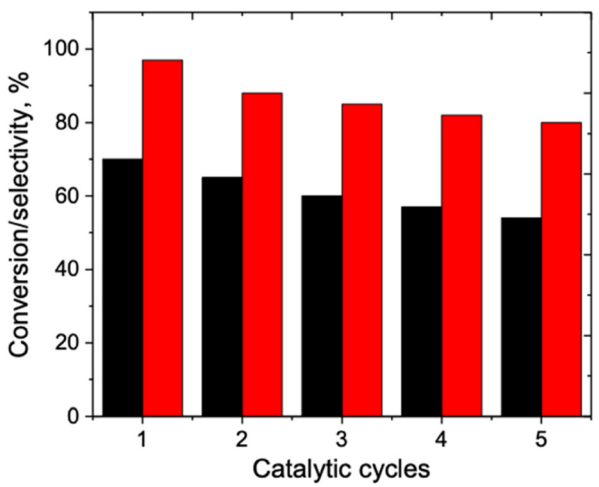

Fig. 8 Catalyst performance chart, 170 °C, 1 h. Conversion and selectivity charted by black and red bars, respectively.

Plausible mechanistic insights may adequately describe the experimental data of the studied process as shown in Scheme 2.

The reaction is promoted by the coexistence of Brønsted and Lewis acidic sites on the catalyst surface, which is consistent with the reported high activity in literature.[12,13] Although surface area can influence heterogeneous reactions, in this system acidity appears to be the dominant factor.[37] On the basis of this background, the acetalization can be described under the herein investigated conditions by six consecutive steps (**A–F**). Step **A** is the initial physisorption of furfural (FF) on the catalyst surface, a process likely enhanced by the hydrophobic character of the CSR support favored, in addition, by the carboxylic groups of the immobilized Ni(II) oxalate (Scheme 2). In fact, the metal oxalate moiety of the material provides most part of the catalyst acidity, both Brønsted and Lewis (Table 2 and Fig. S1). The last feature, in turn, may also be responsible for the improvement of the adsorption of electron-abundant FF.

Once adsorbed, the carbonyl oxygen of FF is activated either by protonation at a Brønsted site or by coordination to a Lewis-acidic Ni center, which increases the electrophilicity of the carbonyl carbon (A → A′). In addition, immobilized Ni-oxalate species may contribute to FF activation. Proton groups on the CSR support and partially deprotonated oxalate ligands ($HC_2O_4^-$) can donate protons, forming tetra-dentate Ni $(HC_2O_4)_2$ complexes under water-free conditions. In these complexes, two covalent C–O–Ni bonds and two C–OH–Ni interactions are established, potentially enhancing FF protonation.

The presence of Brønsted sites on all three materials (NiOx, 2.5%NiOx@CSR, and CSR) is confirmed by Py-GC (Table 2) and DRIFT-Py (Fig. S1) analysis. Further support comes from DRIFT spectra (Fig. 9). Bulk NiOx and 2.5%NiOx@CSR show a strong O–H stretching band at 3380 cm^{-1}, particularly pronounced in NiOx, corresponding to the hydroxyl groups of oxalate ligands. This signal is absent in the spectrum of pristine CSR.[38] A second prominent peak at 1614 cm^{-1}, strong in NiOx and medium in NiOx@CSR, corresponds to the asymmetric vibration of the carboxylate ion ($HC_2O_4^-$), indicating preservation of the carboxylate resonance in the complexes. A third doublet peak at 1312 cm^{-1} is assigned to the symmetric vibration of the oxalate ν–O═C–O– group. The final major band at 820 cm^{-1} is attributed to combined ν(C–C) + δ(OCO) vibrations. Minor peaks between 3100–3000 cm^{-1} in 2.5% NiOx@CSR and CSR correspond to C–H stretching of condensed aromatic structures in the carbon char. Finally, a signal at 990 cm^{-1}, present in both 2.5%NiOx@CSR and CSR, may indicate isolated hydrogen atoms on substituted aromatic rings.[39] A nucleophilic alcohol molecule then attacks the activated carbonyl, breaking the C═O π-bond and forming a hemiacetal intermediate (**B**).

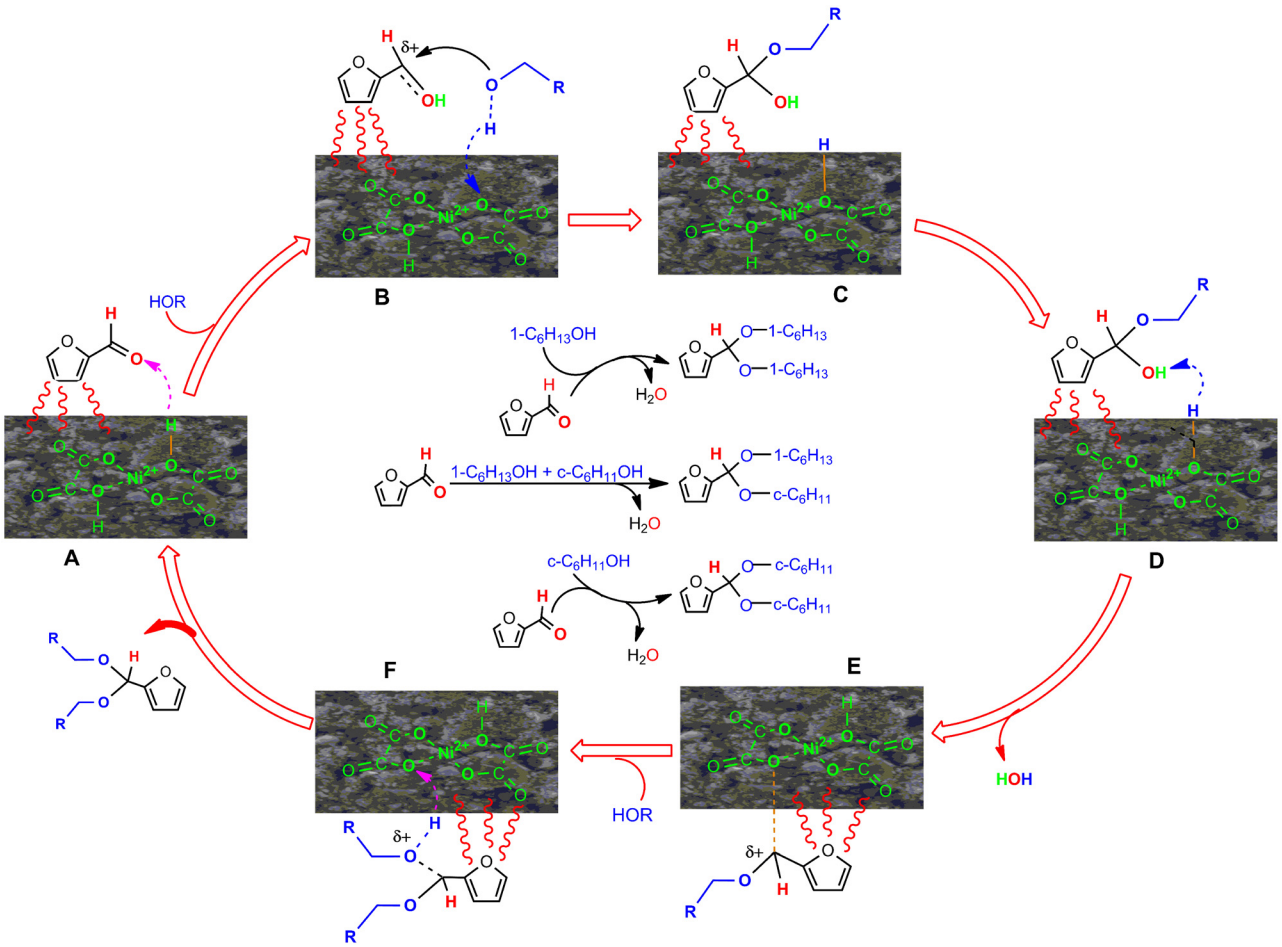

Scheme 2 Mechanistic insights into the solvent-free FF acetalization on 2.5%NiOx@CSR in the C6 aliphatic and alicyclic mono-alcohols medium.

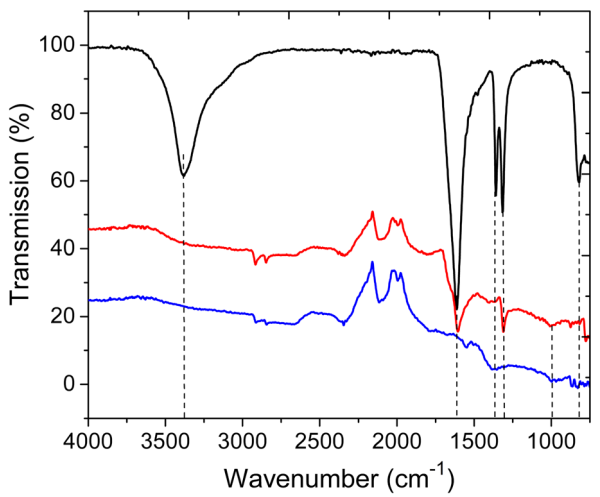

Fig. 9 DRIFT spectra of NiOx (black), 2.5%NiOx@CSR (red) and pristine CSR (blue).

Restoration of the catalyst's acidic state completes hemiacetal formation (**C**). Protonation of the hemiacetal hydroxyl converts it into a good leaving group (water), generating a resonance-stabilized oxonium ion (**D** → **E**).[40] A second alcohol molecule attacks the oxonium ion to give a protonated acetal (**F**). Finally, deprotonation—facilitated by a basic site or the oxalate moiety associated with the deposited Ni species—yields the neutral acetal product and regenerates the acidic catalyst site (return to **A**). This mechanistic sequence accounts for formation of the two individual diacetals (FF-1-hexanol and FF-*c*-hexanol) and the hybrid diacetal observed when both alcohols are present. The pronounced hydrophobicity of the CSR support is an additional advantage: it helps expel the water formed in the reaction from the local reaction zone, shifting the equilibrium toward acetal formation and reducing product hydrolysis.[41] Results herein correlate well with those recently reported for FF acetalization, broad range of alcohols (C1–C8) and silica-supported Fe and Co oxalates.[21] In both cases metal oxalates, either supported onto silica gel or carbon char, revealed high catalytic efficiency even for longer chain (≥C5) mono-alcohols (Table S2). Hemiacetals were exclusively detected as main products for the alcohols ranging from C5 and up to C8 in reactions catalyzed by silica-supported metal oxalates. In contrast, the reaction continued to the formation of diacetals (even in case of 1-C6OH and *c*-C6OH alcohols) for the Ni-carbonaceous material. Moreover, in case of Fe- or

CoOx@silica, in contrast to NiOx@CSR, no hybrid acetals were observed when mixtures of FF and ≥C5 alcohols were explored.[21] These relevant findings may be related to the decisive impact of support nature (*e.g.* physico-chemical properties, hydrophobicity and acidity).

Results have also been compared to literature data as shown in Table S2.[21,34,42–50] According to the comparative analysis, optimum results (in terms of reaction performance and time) were obtained when the reaction systems comprised: (i) catalysts, based on noble (Pd, Ru) metals deposited either on inorganic (SiO_2 or molecular sieves) or organic (carbon) supports featuring mild to strong acidity; (ii) non-branched (preferably low weight C1–C4) alcohols; (iii) low content (<1 M) of FF in order to sustain the acceptable level of selectivity (Table S2).

In line with the data reported herein and literature reports, process performance was strongly dependent on the spatial structure of taken alcohols. Switching from the linear mono-alcohols to the iso (*e.g.* i-PrOH) or cyclic (*e.g.* *c*-$C_6H_{11}OH$) ones critically hampers catalytic activity (Table S2).[34,47,48] Last observation undoubtedly points out the mutual influence of the reaction substrates on the studied process efficiency. Table S2 also pointed to a slightly reduced but almost comparable performance of NiOx@CSR to most effective precious metal systems, supporting its potential for practical applications.

Experimental

Materials and methods

Furfural ($C_5H_4O_2$) and the primary alcohols 1-hexanol (1-$C_6H_{13}OH$), cyclohexanol (*c*-$C_6H_{11}OH$), *n*-hexane (C_6H_{14}), and methanol (MeOH) were purchased from Sigma-Aldrich and Panreac. All chemicals were of analytical grade and used without further purification. Oxalic acid dihydrate ($C_2H_2O_4{\cdot}2H_2O$) and nickel(II) chloride tetrahydrate ($NiCl_2{\cdot}4H_2O$), both >99% purity, were obtained from Sigma-Aldrich.

The post-consumer plastic mixture was sourced from the reject fraction of a municipal solid waste treatment plant. Its composition was 55.0% polypropylene (PP), 8.6% high-impact polystyrene (HIPS), 10.1% expanded polystyrene (EPS), and 27.7% polyethylene (PE) film. The mixture was crushed to <1 mm and subjected to pyrolysis in a Nabertherm horizontal tubular furnace under nitrogen flow (50 L h^{-1}). The temperature was increased from room temperature to 500 °C at 10 °C min^{-1}, followed by a 90 min isothermal hold. The resulting plastic-derived carbon char (CSR) was dried overnight at 100 °C, cooled in a desiccator, and stored in airtight containers until use.

Catalysts preparation

Key steps for the preparation of supported Ni(II) oxalate (NiOx) catalyst are shown in Fig. 10. First, the metal salt solution was stirred at room temperature for 30 min and then added dropwise to 2.5 g of dry CSR under gentle mixing. The resulting slurry was dried overnight at 80 °C to yield a dispersed solid. 0.50 g (4.0 mmol, 4 eq. *vs.* Ni) of oxalic acid were subsequently dissolved in 2.5 mL of methanol and stirred for 1 h at room temperature. This solution was added dropwise to dry $NiCl_2$/CSR composite and dried again at 80 °C for 12 h. The catalyst precursor was washed three times with 15 mL methanol; each cycle consisted of 15 min stirring followed by centrifugation at 1000 rpm for 3 min and removal of the supernatant. The wet catalyst was then dried at 80 °C for 12 h and stored in a desiccator until characterization and testing.

Catalyst characterization

Textural properties were determined by N_2 physisorption at −196 °C using a Micromeritics ASAP 2000 instrument. Samples were degassed under vacuum at 100 °C for 24 h prior to analysis. Specific surface area was calculated using the Brunauer–Emmett–Teller (BET) method; pore size distribution and total pore volume were derived from the Barrett–Joyner–Halenda (BJH) model, and average pore diameter was estimated as $4V_p/S_{BET}$.

Powder X-ray diffraction (XRD) patterns were recorded on a Bruker D8 Discover diffractometer (40 kV, 40 mA) with Cu Kα radiation (λ = 1.54 Å), using a scan speed of 0.5° min^{-1} over $0.5° < 2\Theta < 5°$ for low-angle measurements.

Surface acidity was evaluated by pyridine-adsorbed diffuse reflectance FTIR spectroscopy (Py-DRIFT) using an ABB 3000MB instrument equipped with a PIKE Technologies MIRacle™ Single Reflection ATR environmental chamber under a 20 mL min^{-1} air flow. Samples were pre-treated at 100 °C for 1 h (higher temperatures were avoided to prevent Ni-oxalate decomposition), saturated in pyridine vapor at 90 °C for 20 min, and analyzed on a PerkinElmer FTIR Spectrum 3. Same instrument was also employed for DRIFT measurements of NiOx, 2.5%NiOx@CSR and CSR materials.

Quantitative acidity measurements were obtained *via* pulse chromatographic titration at 300 °C using pyridine (PY) and 2,6-dimethylpyridine (DMPY) in cyclohexane (0.1 mol L^{-1} and 0.7 mol L^{-1}, respectively) on a Hewlett Packard 5890 Series II gas chromatograph.

Morphological analysis was conducted by scanning electron microscopy (SEM) using a JEOL JSM 6300. X-ray photoelectron spectroscopy (XPS) was performed with a Phoibos 150 MCD spectrometer (Specs, Berlin, Germany) using an Al Kα source ($h\nu$ = 1486.6 eV) operated at 400 W; C 1s at 284.6 eV served as the reference.

Thermal stability was assessed by thermogravimetric analysis (TGA) using a TGA/DSC 1 STAR system (Mettler Toledo). Samples were heated from 30 to 700 °C at 10 °C min^{-1} under nitrogen.

Catalytic tests

Microwave (MW)-assisted reactions were performed in 10 mL Pyrex batch reactors (1 cm diameter × 10 cm height) equipped with magnetic stirring. The total reaction volume was fixed at

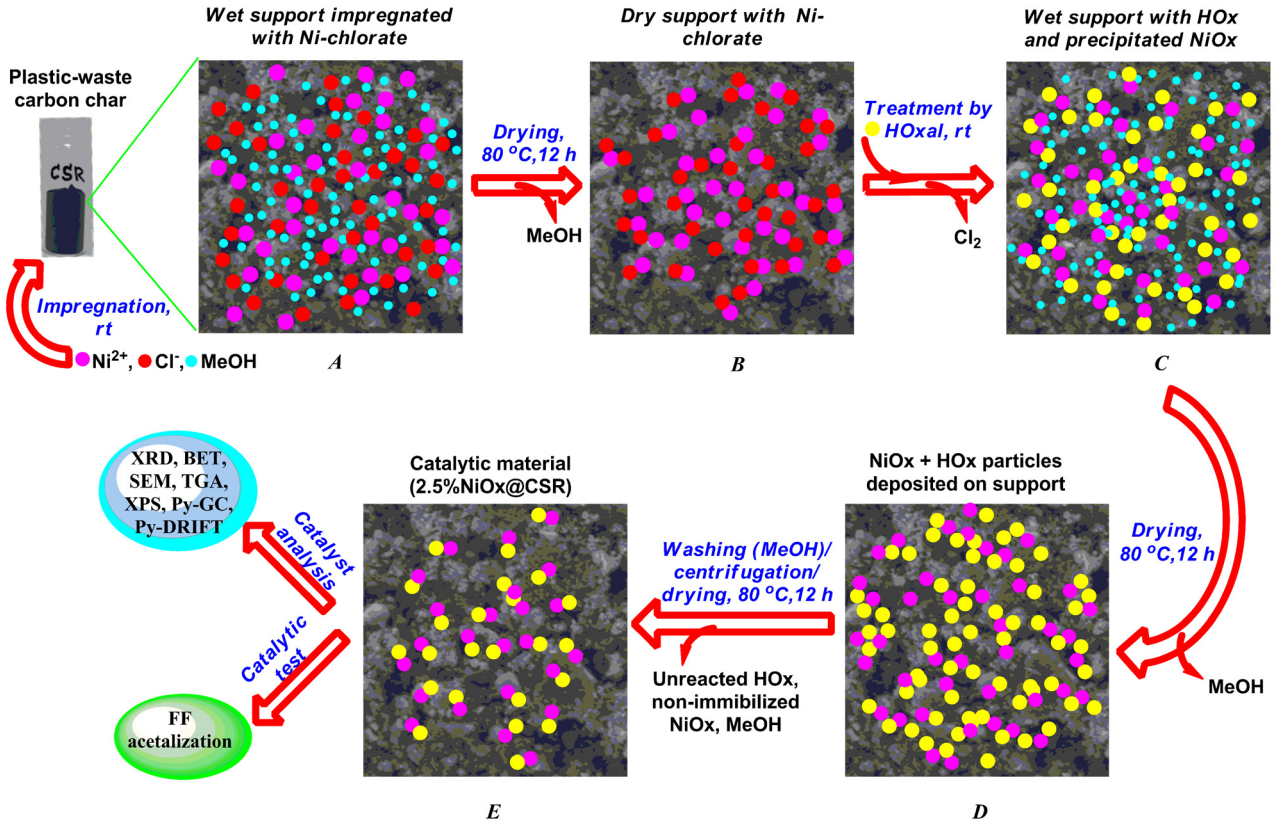

Fig. 10 Preparation of 2.5%NiOx@CSR catalytic material.

2 mL. Reaction temperatures ranged from 130 to 170 °C and reaction times from 0.5 to 2 h.

In a standard experiment, 0.083 mL (1.0 mmol) of furfural (FF) was dissolved in 2 mL of alcohol (1-hexanol and/or cyclohexanol), providing a 0.5 M FF solution. Then, 0.05 g of catalyst was added, the reactor was sealed, placed in the microwave cavity, and the reaction initiated under stirring at the selected temperature and time.

After completion, the mixture was filtered through a syringe microfilter. The filtrate was diluted 1 : 1 (v/v) with an internal standard solution (0.117 M toluene in acetonitrile). Samples were analyzed by gas chromatography (GC) using an HP Series II GC equipped with an EQUITY™-1 fused-silica capillary column (60 m × 0.25 mm × 0.25 μm) and flame ionization detector (FID).

Product identification was confirmed by gas chromatography–mass spectrometry (GC-MS) using a 5977B MSD instrument.

Furfural conversion (C %) and product (diacetals) selectivity (S %) were calculated using the following equations:

$$\text{Conv FF (mol\%)} = \frac{n_i(\text{FF}) - n_f(\text{FF})}{n_i(\text{FF})} \times 100$$

$$\text{Sel (mol\%)} = \frac{n(FF) \text{ in a certain product}}{n(FF) \text{ converted}} \times 100$$

Conclusions

A heterogeneous 2.5%NiOx@CSR catalyst, generated *via in situ* formation and deposition of Ni(II) oxalate on plastic-waste-derived carbon char, was prepared, characterized and evaluated in the acetalization of furfural (FF) with 1-hexanol and cyclohexanol. FF conversions of 60–65% and TON of 150 were achieved, together with excellent selectivities (95–98%), and the material exhibited satisfactory reusability over five consecutive reaction cycles. A notable enhancement in process performance was observed when alcohols were employed as mixtures *ca.* 40% increase in overall yield. Under these conditions, a hybrid furfurylhexyl/cyclohexyl diacetal was also formed in addition to the individual products (furfuryl-*n*-hexyl diacetal and furfurylcyclohexyl diacetal). This result demonstrates that mixed-alcohol feedstocks can be employed to access hybrid FF diacetals containing alkyl groups derived from different alcohols.

Process efficiency can be further improved by introducing *n*-hexane as a co-solvent, especially pronounced at lower temperatures and in reaction media based on secondary alcohols (*e.g.*, cyclohexanol). In this case, the presence of 40–45 vol% of *n*-hexane at 150–170 °C increased the yield of furfurylcyclohexyl diacetal by a factor of 5–6 compared to *n*-hexane-free conditions.

Overall, the study illustrates that the NiOx-modified carbon supports derived from plastic waste are suggested as efficient,

robust, tunable and cheap catalysts for the sustainable production of furfural-based diacetals, including novel hybrid structures accessible from mixed-alcohol systems.

Author contributions

Conceptualization: AP, AB, RL; data curation: AP, RL; formal analysis: AP, AB, RL; funding acquisition: AB, RL; investigation: AP, SPH; methodology: AP, AB, RL; project administration: AB, RL; resources: AB, RL; supervision: AB, RL, SPH; writing: original draft: AP, SPH; writing: review & editing: AB, RL.

Conflicts of interest

There are no conflicts to declare.

Data availability

The data supporting this article have been included as part of the supplementary information (SI). Supplementary information is available. See DOI: https://doi.org/10.1039/d5dt02838h.

Acknowledgements

This work has been funded by the European Union – Health and Digital Executive Agency (HADEA), project SusPharma grant agreement No 101057430. Views and opinions expressed are however those of the authors only and do not necessarily reflect those of the European Union or the Health and Digital Executive Agency. Neither the European Union nor the granting authority can be held responsible for them. Members of Nanoval Group (University of Cordoba) are sincerely acknowledged for their audience. The help of Bryan F. Rivadeneira-Mendoza in carrying out analysis and results interpretation is kindly appreciated.

References

1 J. He, Q. Qiang, L. Bai, W. Su, H. Yu, S. Liu and C. Li, *Ind. Chem. Mater.*, 2024, **2**, 30.
2 D. Nedumaran and A. Pandurangan, *Microporous Mesoporous Mater.*, 2013, **169**, 25.
3 M. J. Climent, A. Velty and A. Corma, *Green Chem.*, 2002, **4**, 565.
4 P. G. M. Wuts and K. Michigan, Protection for the Carbonyl Group, in *Greene's Protective Groups in Organic Synthesis*, Academic Press, New York, 5th edn, 2014, pp. 554.
5 I. P. Jakopović, S. Kapić, S. Alihodžić and V. Šunjić, Ethers from esters; from exceptional transformation to synthetic method, *ARKIVOC*, 2015, (i), 300–326, and references cited therein.
6 Y. Wang, Q. Cui, Y. Guan and P. Wu, *Green Chem.*, 2018, **20**, 2110.
7 K. Sakoda, S. Yamaguchi, T. Mitsudome and T. Mizugaki, *JACS Au*, 2022, **2**, 665.
8 Y.-L. Lin, N.-Y. Zheng, H.-J. Cheng and C.-C. Chang, *Fuel*, 2024, **367**, 131349.
9 N. H. Arbain and J. Salimon, *E-J. Chem.*, 2011, **8**(S1), S33–S40.
10 J.-L. Dong, L.-S.-H. Yu and J.-W. Xie, *ACS Omega*, 2018, **3**, 4974.
11 M. Hatano, C. Nishioka, A. Mimura, R. Kimura, Y. Okuda, T. Yamada and K. Sakata, *Synlett*, 2023, 2508.
12 Z. Chen, Y. Wen, Y. Fu, H. Chen, M. Ye and G. Luo, *Synlett*, 2017, 981.
13 S. Esfandmaz, N. Chaibakhsh, Z. Moradi-Shoeili and A. Mohammadi, *Sustainable Chem. Pharm.*, 2018, **8**, 82.
14 X. Wang, X. Liang, J. Li and Q. Li, *Appl. Catal., A*, 2019, **576**, 85.
15 A. Patil, S. Shinde, S. Kamble and C. V. Rode, *Energy Fuels*, 2019, **33**, 7466.
16 Z. Ma, L. Wang, Z. Wang, H. Cui, E. Tang, H. Hou, G. Xu, T. Song and Q. Wang, *ChemCatChem*, 2024, **16**(23), e202401072.
17 A. Bazargan, C. W. Hui and G. McKay, *Adv. Polym. Sci.*, 2015, **266**, 1.
18 Z. Yang, C. Lei, X. Zhao, R. Liu, H. Wei, Y. Ma, S. Meng, Q. Cao, J. Wei and X. Wang, *ChemSelect*, 2017, **2**, 9377.
19 R. Mariscal, P. Maireles-Torres, M. Ojeda, I. Sadaba and M. L. Granados, *Energy Environ. Sci.*, 2016, **9**, 1144.
20 Q. Liu, X. Zhang, Q. Zhang, Q. Liu, C. Wang and L. Ma, *Energy Fuels*, 2020, **34**(6), 7149.
21 A. Pokutsa, K. Rydel-Ciszek, A. M. Balu and R. Luque, *Biofpr*, 2025, DOI: 10.1002/bbb.70097.
22 C. E. Brewera, V. J. Chuang, C. A. Masiello, H. Gonnermann, X. Gao, B. Dugan, L. E. Driver, P. Panzacchi, K. Zygourakis and C. A. Davies, *Biomass Bioenergy*, 2014, **66**, 176.
23 E. Bar-Ziv and I. I. Kantorovich, *Prog. Energy Combust. Sci.*, 2001, **27**, 667.
24 A. Rosencwaig, G. K. Wertheim and H. J. Guggenheim, *Phys. Rev. Lett.*, 1971, **27**, 479.
25 P. Babar, K. Patil, V. Karade, K. Gour, A. Lokhande, S. Pawar and J. H. Kim, *ACS Appl. Mater. Interfaces*, 2021, **44**, 52620.
26 S. Chenakin and N. Kruse, *Appl. Surf. Sci.*, 2020, **515**, 146041.
27 B. F. Rivadeneira-Mendoza, L. S. Quiroz-Fernández, F. da Silva, R. Luque, A. M. Balu and J. M. Rodríguez-Díaz, *Environ. Sci.:Nano*, 2024, **11**, 1543.
28 S. P. Chenakin, R. Szukiewicz, R. Barbosa and N. Kruse, *J. Electron Spectrosc. Relat. Phenom.*, 2016, **209**, 66.
29 D. G. Gil-Gavilán, J. Amaro-Gahete, R. Rojas-Luna, A. Benítez, R. Estevez, D. Esquivel, F. M. Bautista and F. J. Romero-Salguero, *ChemCatChem*, 2024, **16**, e202400251.

30 S. Chenakin and N. Kruse, *J. Phys. Chem. C*, 2019, **123**, 30926.
31 N. N. M. Borel, J. Foba-Tendo, D. M. Yufanyi, E. P. Etape, J. N. Eko and L. J. Ngolui, *J. Appl. Chem.*, 2014, 767695.
32 B. Małecka, A. Małecki, E. Drożdż-Cieśla, L. Tortet, P. Llewellyn and F. Rouquerol, *Thermochim. Acta*, 2007, **466**, 57–62.
33 F. M. Bautista, J. M. Campelo, A. Garcia, D. Luna, J. M. Marinas, A. A. Romero, J. A. Navio and M. Macias, *J. Catal.*, 1994, **145**, 107.
34 A. Bailey, T. Bere, T. E. Davies, S. H. Taylor and A. E. Graham, *ACS Sustainable Chem. Eng.*, 2022, **10**, 13759.
35 C. Gabriel, S. Gabriel, E. H. Grant, B. S. I. Halstead and D. M. P. Mingos, *Chem. Soc. Rev.*, 1998, **27**, 213.
36 Y.-L. Lin, N.-Y. Zheng, H.-J. Cheng and C.-C. Chang, *Fuel*, 2024, **367**, 131349.
37 J. M. R. Caballero, S. Saravanamurugan, P. M. Torres and A. Riisager, *Catal. Today*, 2014, **234**, 233.
38 M. Niculescu, M.-C. Pascariu, A. Racu and B.-O. Taranu, *J. Serb. Chem. Soc.*, 2024, **89**, 1475.
39 X. Wang, X. He and X. Wang, *J. Appl. Sci.*, 2023, **13**, 5162.
40 A. Garcia, D. A. L. Otte, W. A. Salamant, J. R. Sanzone and K. A. Woerpel, *J. Org. Chem.*, 2015, **80**, 4470.
41 D. M. Arvelo, J. Comer, J. Schmit and R. Garcia, *ACS Nano*, 2024, **18**, 18683.
42 M. S. Hosseini, M. Masteri-Farahani, M. Ghahremani and N. Forouzeshfar, *J. Phys. Chem. Solids*, 2021, **150**, 109846.
43 M. J. da Silva, C. J. Ribeiro, E. N. de Araújo and M. Torteloti, *Processes*, 2023, **11**, 2220.
44 E. G. Tane, Z. Ruiz-Bernal, C. Lopez-Cerrano, M. A. Lillo-Rodenas and M. C. Roman-Martinez, *Catal. Today*, 2025, **458**, 115366.
45 S. U. Raut and P. R. Bhagat, *Biomass Convers. Biorefin.*, 2023, **13**, 7737–7754.
46 R. Kosydar, E. Lalik, J. Gurgul, T. Szumełda and A. Drelinkiewicz, *Int. J. Hydrogen Energy*, 2024, **60**, 293.
47 M. J. da Silva and M. G. Teixeira, *Mol. Catal.*, 2018, **461**, 40.
48 Q. Fang, H. Du, X. Liu and Y. Ding, *Catal. Today*, 2024, **442**, 114936.
49 X. Guo, H. Wu, P. Wu, M. He and Y. Guan, *Green Energy Environ.*, 2023, **8**, 519.
50 J. Ratthiwal, N. Lazarro, A. A. Romero, S. M. Osman, P. Reubroycharoen and R. Luque, *Fuels*, 2023, **332**, 126049.